

# Designing Novel Cognitive Diagnosis Models via Evolutionary Multi-Objective Neural Architecture Search

Shangshang Yang, Haiping Ma, Cheng Zhen, Ye Tian, Limiao Zhang, Yaochu Jin, *Fellow, IEEE*, and Xingyi Zhang, *Senior Member, IEEE*

**Abstract**—Cognitive diagnosis plays a vital role in modern intelligent education platforms to reveal students’ proficiency in knowledge concepts for subsequent adaptive tasks. However, due to the requirement of high model interpretability, existing manually designed cognitive diagnosis models hold too simple architectures to meet the demand of current intelligent education systems, where the bias of human design also limits the emergence of effective cognitive diagnosis models. In this paper, we propose to automatically design novel cognitive diagnosis models by evolutionary multi-objective neural architecture search (NAS). Specifically, we observe existing models can be represented by a general model handling three given types of inputs and thus first design an expressive search space for the NAS task in cognitive diagnosis. Then, we propose multi-objective genetic programming (MOGP) to explore the NAS task’s search space by maximizing model performance and interpretability. In the MOGP design, each architecture is transformed into a tree architecture and encoded by a tree for easy optimization, and a tailored genetic operation based on four sub-genetic operations is devised to generate offspring effectively. Besides, an initialization strategy is also suggested to accelerate the convergence by evolving half of the population from existing models’ variants. Experiments on two real-world datasets demonstrate that the cognitive diagnosis models searched by the proposed approach exhibit significantly better performance than existing models and also hold as good interpretability as human-designed models.

**Index Terms**—Cognitive diagnosis models, neural archi-

Manuscript received –. This work was supported in part by the National Key Research and Development Project under Grant 2018AAA0100105 and 2018AAA0100100, in part by the National Natural Science Foundation of China under Grant 61822301, 61876123, 61906001, 62136008, U21A20512, and U1804262, in part by the Anhui Provincial Natural Science Foundation under Grant 1808085J06 and 1908085QF271, in part by the Collaborative Innovation Program of Universities in Anhui Province under Grant GXXT-2020-013, and in part by the State Key Laboratory of Synthetical Automation for Process Industries under Grant PAL-N201805 (*Corresponding authors: Limiao Zhang and Xingyi Zhang*).

S. Yang and X. Zhang is with the Key Laboratory of Intelligent Computing and Signal Processing of Ministry of Education, School of Artificial Intelligence, Anhui University, Hefei 230039, China (email: yangshang0308@gmail.com; xyzhanghust@gmail.com).

C. Zhen, Y. Tian, and H. Ma are with the Key Laboratory of Intelligent Computing and Signal Processing of Ministry of Education, Institutes of Physical Science and Information Technology, Anhui University, Hefei 230601, China (email: zhencheng0208@gmail.com; field910921@gmail.com; hpma@ahu.edu.cn).

L. Zhang is with Information Materials and Intelligent Sensing Laboratory of Anhui Province, Anhui University, Hefei, 230601, Anhui, China (email: zhanglm@ahu.edu.cn).

Y. Jin is with the Faculty of Technology, Bielefeld University, Bielefeld 33619, Germany (email: yaochu.jin@uni-bielefeld.de).

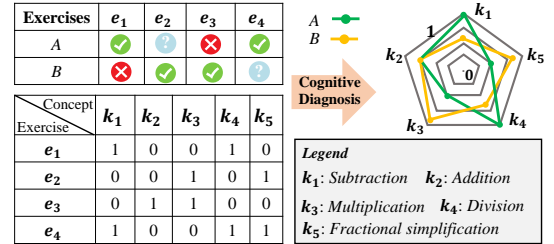


Fig. 1: The illustration of cognitive diagnosis process. The response records of students  $\{A, B\}$ , and the exercise-concept relational matrix ( $Q$ -matrix) are shown in the left, while the top right gives the diagnosis results.

ecture search, evolutionary algorithm, multi-objective optimization, genetic programming, model interpretability.

## I. INTRODUCTION

Cognitive diagnosis (CD) in the field of intelligent education [1], [2] aims to reveal students’ proficiency in specific knowledge concepts according to their historical response records of answering exercises and the exercise-concept relational matrix (termed  $Q$ -matrix) [3]. Fig. 1 gives an illustrative example of CD, where students  $\{A, B\}$  have practiced a series of exercises (i.e.,  $\{e_1, e_3, e_4\}$  and  $\{e_1, e_2, e_3\}$ ), and got corresponding responses. Based on the records and  $Q$ -matrix, the students’ knowledge proficiency in each concept can be obtained through CD. By doing so, there is a wide range of intelligent education tasks, such as personalized exercise recommendation [4] and targeted training [5], which can benefit from the students’ diagnosis results.

With the rising demand for cognitive diagnosis models (CDMs) in online education platforms, many researchers developed various CD approaches, which are generally grouped into two types. The first genre of approaches is mainly proposed by researchers in educational psychology. Their designed CDMs usually rely on simple handcrafted functions to model student-exercise interactions and portray the student learning ability in a one-dimensional vector or other manners. The representatives include *Item Response Theory* (IRT) [6], *Deterministic Input, Noisy ‘And’ gate* (DINA) [7], *Multidimensional IRT* (MIRT) [8], and *Matrix Factorization* (MF) [9]. The sec-

ond genre of ones [10]–[14] is based on neural networks (NNs), where the student learning ability is portrayed by an inner latent vector. The representatives contain *Neural Cognitive Diagnosis* (NCD) [11], *Prerequisite Attention model for Knowledge Proficiency diagnosis* (PAKP) [15], and *Relation map driven Cognitive Diagnosis* (RCD) [13].

As the critical components of CDMs, diagnostic functions are mainly responsible for predicting student exercising scores by integrating three types of input vectors (i.e., student/exercise/concept-related input vector) in a highly interpretable manner. To pursue high model interpretability, existing CDMs' diagnostic functions are desired to hold simple architectures. For example, IRT [6] and MF [9] utilize the simple logistic function and inner-product respectively as their diagnostic functions. However, there exist two kinds of problems for these simple handcrafted diagnostic functions. Firstly, simple diagnostic functions' architectures disable CDMs from modeling complex relationships between students and exercises well [16], failing to meet the demands of modern education systems containing a large quantity of student exercising data. Secondly, the design of existing diagnostic functions heavily relies on researchers' knowledge of both educational psychology and NNs [11], which is labor-intensive and needs a lot of trial-and-error. And the human design bias may limit the emergence of novel diagnostic functions to some extent. Furthermore, recent CD approaches [13]–[15] put less focus on the architecture design of diagnostic functions but on enhancing the input vectors for high performance, which hinders the development of CDMs to some extent.

For the above reasons, this paper aims to develop novel CDMs by automatically designing effective diagnostic function architectures. Since Zoph and Le [17] proposed to search neural architectures for image tasks, neural architecture search (NAS) [18]–[20] has been widely applied to many research fields and achieved significant success [21]–[23]. Among various search strategies of NAS, including reinforcement learning [24] and gradient optimization [21], [25], evolutionary algorithms (EAs), especially multi-objective evolutionary algorithms (MOEAs), have shown a more powerful ability to search [18]. Moreover, compared to other NAS approaches, MOEA-based NAS approaches [26] are superior in getting out of local optima and presenting trade-offs among multiple objectives, where many architectures holding different attributes can be found in a single run. The representative approaches include *Neural Architecture Search using Multi-Objective Genetic Algorithm* (NSGA-Net) [27], and *Lamarckian Evolutionary algorithm for Multi-Objective Neural Architecture Design* (LEMONADE) [24]. However, existing NAS approaches cannot be applied to CD due to the difference in search space between CD and other tasks, and different search space generally needs different MOEAs [26], whose representations and genetic operations are task-tailored [28], further hindering them from being applied to CD.

Therefore, this paper proposes an evolutionary multi-

objective NAS to design novel CDMs (termed EMO-NAS-CD), where an expressive search space is first devised and multi-objective genetic programming (MOGP) is employed to explore the search space to develop high-performance CDMs with good interpretability. Specifically, our main contributions are as follows:

- 1) This paper is the first NAS work to design CDMs, which explores the search space design and search strategy design of NAS. Regarding the search space, we first design an expressive search space for the NAS task of CD (NAS-CD) by summarizing existing diagnostic function architectures. Within, each candidate architecture is denoted by a general model, which takes at most three given types of input vectors as input nodes. Then, regarding the search strategy, we propose MOGP to explore the search space by solving a bi-objective problem of NAS-CD, which maximizes the objectives of model performance and interpretability simultaneously.
- 2) In the MOGP design, we first transform architectures under the search space into tree architectures and then encode them by trees for easy optimization, which can avoid the optimization difficulties of vector-based encoding (e.g., the problem of variable-length encoding). Based on four sub-genetic operations, a tailored genetic operation is devised for effective offspring generation in the MOGP. Besides, to accelerate the MOGP's convergence, we further design a prior knowledge-based initialization strategy to evolve partial individuals of the population from existing CDMs' variants.
- 3) To validate the effectiveness of the proposed EMO-NAS-CD, we compare it with some representative CDMs on two popular education datasets. Experimental results show that EMO-NAS-CD can find a set of architectures to build CDMs, which present trade-offs between interpretability and performance. The found architectures hold both significantly better prediction performance and good interpretability. Moreover, we verify the effectiveness of the suggested genetic operation as well as the initialization strategy, and we also demonstrate the superiority of the devised model interpretability objective over the common model complexity.

The rest of this paper is as follows. Section II reviews existing CD approaches and presents the motivation for this work. Section III introduces the proposed search space. Section IV presents the details of the proposed approach. The experiments are shown in Section V, and we give conclusions and future work in Section VI.

## II. PRELIMINARIES AND RELATED WORK

### A. Preliminaries of Cognitive Diagnosis Task

Formally, there are  $N$  students,  $M$  exercises, and  $K$  knowledge concepts in an intelligent education platform for the cognitive diagnosis task, which can be represented by  $S = \{s_1, s_2, \dots, s_N\}$ ,  $E = \{e_1, e_2, \dots, e_M\}$ , and

$C = \{c_1, c_2, \dots, c_K\}$ , respectively. Besides, there is commonly an exercise-concept relation matrix  $Q = (Q_{jk} \in \{0, 1\})^{M \times K}$ ,  $Q$ -matrix, to depict the relationship between exercises and knowledge concepts, where  $Q_{jk} = 1$  means the exercise  $e_j$  contains the knowledge concept  $c_k$  and  $Q_{jk} = 0$  otherwise.  $R_{log}$  is used to denote the students' exercising response logs and it can be represented by a set of triplets  $(s_i, e_j, r_{ij})$ , where  $s_j \in S$ ,  $e_j \in E$ , and  $r_{ij} \in \{0, 1\}$  refers to the response score of student  $s_i$  on exercise  $e_j$ . Here  $r_{ij} = 1$  indicates the answer of student  $s_i$  on  $e_j$  is correct and  $r_{ij} = 0$  otherwise.

Based on the students' response logs  $R_{log}$  and  $Q$ -matrix, the cognitive diagnosis task mines the students' proficiency in knowledge concepts by building a model  $\mathcal{F}$  to predict the students' exercising score. To predict the score of student  $s_i$  on exercise  $e_j$ , the model  $\mathcal{F}$  can take three types of inputs, including the student-related feature vector  $\mathbf{h}_S \in R^{1 \times D}$ , the exercise-related feature vector  $\mathbf{h}_E \in R^{1 \times D}$ , and the knowledge concept-related feature vector  $\mathbf{h}_C \in R^{1 \times K}$ , which can be obtained by

$$\begin{aligned} \mathbf{h}_S &= \mathbf{x}_i^S \times W_S, W_S \in R^{N \times D} \\ \mathbf{h}_E &= \mathbf{x}_j^E \times W_E, W_E \in R^{M \times D} \\ \mathbf{h}_C &= \mathbf{x}_j^E \times Q = (Q_{j1}, Q_{j2}, \dots, Q_{jK}) \end{aligned}, \quad (1)$$

where  $D$  is the embedding dimension (usually equal to  $K$  for consistency),  $\mathbf{x}_i^S \in \{0, 1\}^{1 \times N}$  is the one-hot vector for student  $s_i$ ,  $\mathbf{x}_j^E \in \{0, 1\}^{1 \times M}$  is the one-hot vector for exercise  $e_j$ , and  $W_S$  and  $W_E$  are trainable matrices in the embedding layers. Then, the model  $\mathcal{F}$  outputs the predicted response  $\hat{r}_{ij}$  as  $\hat{r}_{ij} = \mathcal{F}(\mathbf{h}_S, \mathbf{h}_E, \mathbf{h}_C)$ , where  $\mathcal{F}(\cdot)$  is the diagnostic function to combine three types of inputs in different manners. Generally speaking, after training the model  $\mathcal{F}$  based on students' response logs, each bit value of  $\mathbf{h}_S$  represents the student's proficiency in the corresponding knowledge concept.

## B. Related Work on Cognitive Diagnosis

In the past decades, a series of CDMs have been developed based on researchers' experiences in educational psychology and deep neural networks (DNNs), mainly from two perspectives.

1) **Incorporating Richer Input Information:** As introduced above, there are three types of inputs that can be used for the diagnostic function in a CDM, including the student-related vector  $\mathbf{h}_S$ , the exercise-related vector  $\mathbf{h}_E$ , and the knowledge concept-related vector  $\mathbf{h}_C$ . Therefore, the first type of approaches aims to incorporate richer context information or other information into these input vectors to boost the diagnostic function inputs for improving the prediction performance.

To achieve this, Zhou *et al.* [12] proposed *Educational context-aware Cognitive Diagnosis* (ECD) [12] to model educational context-aware features in student learning. Specifically, the student's educational contexts (e.g., school information, student personal interests, parents' education) are incorporated into the student-related vector  $\mathbf{h}_S$  by a hierarchical attention NN. Then, the

integrated student-related vector  $\mathbf{h}_S$  will be processed by a common diagnostic function. The incorporated educational context information can indeed improve the diagnosis performance of different diagnostic functions, including IRT, MIRT, and NCD.

In [13], Gao *et al.* proposed RCD to incorporate the model inputs with the prior relations between knowledge concepts. To be specific, students, exercises, and concepts are first built as a hierarchical graph. This graph contains a student-exercise interaction map, a concept-exercise correlation map, and a concept dependency map that is extracted from the prior relations between knowledge concepts. Then, a multi-level attention NN is used to achieve node aggregation of the hierarchical graph, and the aggregated node features are used as three input vectors,  $\mathbf{h}_S$ ,  $\mathbf{h}_E$ , and  $\mathbf{h}_C$ , to improve the model performance.

Similarly, Wang *et al.* [14] proposed CDGK (i.e., *Cognitive DiaGnosis by Knowledge concept aggregation*) to incorporate the relations between knowledge concepts into input vectors. Different from RCD, CDGK only builds the graph structure of knowledge concepts according to the dependency among knowledge concepts. Only the leaf nodes in the constructed graph will be used to aggregate the target node's features. Finally, the aggregated knowledge concept features will be taken as the concept-related vector  $\mathbf{h}_C$  used for subsequent diagnosis process.

2) **Designing Diagnostic Functions:** The above CD approaches only focus on incorporating extra information into input vectors, and directly employ existing diagnostic functions to handle the enhanced input vectors for diagnosis. In contrast, the second type of approaches focuses on designing powerful diagnostic functions, which are responsible for combining input vectors in highly interpretable manners.

As the most typical CDM, the diagnostic function of DINA [7] is to first obtain two binary student and concept latent features ( $\boldsymbol{\theta}, \boldsymbol{\beta} \in \{0, 1\}^{1 \times K}$ ) and two exercise latent features (guessing  $g \in R^1$  and slipping  $sl \in R^1$ ) from input vectors. Then, the score of student  $s_i$  on exercise  $e_j$  can be represented as  $\hat{r}_{ij} = g^{1-nt}(1-sl)^{nt}$ , where  $nt = \prod_k \theta_k^{\beta_k}$ . Despite the high interpretability of its diagnostic function, DINA suffers from poor prediction performance in current CD tasks due to its poor scalability on large-scale student exercising data.

As another typical CDM, the diagnostic function of IRT [6] first takes student-related and exercise-related vectors  $\mathbf{h}_S$  and  $\mathbf{h}_E$ , and then transforms them into one student latent feature  $\theta \in R^1$  and two exercise latent features ( $\beta \in R^1$  and  $a \in R^1$ ), respectively. Next, a simple logistic function is applied to the linear transformation of  $\theta$ ,  $\beta$ , and  $a$ , e.g., a simple version is  $Sigmoid(a(\theta - \beta))$  as stated in [10], [11]. Finally, the diagnostic function outputs the predicted scores of the student on exercises.

Similarly, MIRT [8] applies the same logistic function as IRT to the linear transformation of the student latent feature  $\boldsymbol{\theta} \in R^{1 \times K}$ , the exercise latent feature  $\boldsymbol{\beta} \in R^1$ , and the knowledge concept latent feature  $\boldsymbol{\alpha} \in R^{1 \times K}$ .  $\boldsymbol{\theta}$  and

$\alpha$  are equal to  $\mathbf{h}_S$  and  $\mathbf{h}_C$ , and  $\beta$  is transformed from  $\mathbf{h}_E$ . Note that student and knowledge concept latent features in MIRT are multidimensional for the demands of multidimensional data [10]. Finally, its prediction process can be output as  $\hat{r}_{ij} = \text{Sigmoid}(\beta + \sum \alpha \odot \theta)$ . Compared to IRT, MIRT exhibits better performance yet without losing interpretability.

Differently, MF [9] is originally proposed for recommender systems but can be used for CD from the data mining perspective, where students and exercises in CD can correspond to users and items in recommender systems. As demonstrated in [11], the diagnostic function of MF can be modeled as directly applying the inner-product to  $\mathbf{h}_S$  and  $\mathbf{h}_E$ . Finally, its prediction process can be represented by  $\hat{r}_{ij} = \sum \mathbf{h}_S \odot \mathbf{h}_E$ , whose architecture is quite simple yet effective compared to other CDMs.

The most representative approach NCD [11] builds a new diagnostic function with one shallow layer and three fully connected (FC) layers. Firstly, the student latent feature  $\mathbf{f}_S \in R^{1 \times K}$  and two exercise latent features  $\mathbf{f}_{diff} \in R^{1 \times K}$  and  $f_{disc} \in R^1$  are first obtained by

$$\begin{cases} \mathbf{f}_S = \text{Sigmoid}(\mathbf{h}_S) \\ \mathbf{f}_{diff} = \text{Sigmoid}(\mathbf{h}_E) \\ f_{disc} = \text{Sigmoid}(\mathbf{h}_E \times W_{disc}), W_{disc} \in R^{D \times 1} \end{cases}. \quad (2)$$

Then, the shallow layer inspired by MIRT is used to linearly combine the above features and concept-related vector  $\mathbf{h}_C$  as  $\mathbf{y} = \mathbf{h}_C \odot (\mathbf{f}_S - \mathbf{f}_{diff}) \times f_{disc}$ . Afterward, the hidden feature  $\mathbf{y}$  is fed into three FC layers with the monotonicity property to get the final prediction output.

Ma *et al.* proposed *Knowledge-Sensed Cognitive Diagnosis* (KSCD) to diagnose the student's proficiency. Similar to NCD, KSCD's diagnostic function [16] consists of two FC layers followed by one shallow layer. Two FC layers are used to combine the learned knowledge concept features with  $\mathbf{h}_S$  and  $\mathbf{h}_E$ , respectively, for obtaining the enhanced student and exercise features. Then, the shallow layer is used to further combined enhanced features and  $\mathbf{h}_C$  to get the prediction.

### C. Motivation of This Work

Despite the competitive performance of the above CDMs, their diagnosis function architectures are too simple to model complex student-exercise interactions well [16], especially for large-scale student exercising data in current intelligent education systems. Moreover, the design of existing diagnosis function architectures heavily relies on researcher expertise in the domains of both education and NNs, which needs a lot of trial-and-error and thus is labor-intensive and costly [11]. Besides, the human design bias may make some potential yet beyond-human knowledge architectures miss. Therefore, in contrast to current CD approaches focusing on improving model inputs, this paper aims to develop more effective diagnostic function architectures for CD.

As an automated neural architecture design paradigm [21], NAS has been widely used for

TABLE I: 15 Candidate operators.

Notation	Meaning	Syntax	Output shape
<i>Neg</i>	Negative	$-x, x \in R^{1 \times D}$	same
<i>Abs</i>	Absolute value	$ x $	same
<i>Inv</i>	Inverse	$1/(x + \epsilon), \epsilon = 10^{-6}$	same
<i>Square</i>	Square	$x^2$	same
<i>Sqrt</i>	Square root	$\text{sign}(x) \cdot \sqrt{ x  + \epsilon}$	same
<i>Tanh</i>	Tanh function	$\tanh(x)$	same
<i>Sigmoid</i>	Sigmoid function	$\text{sigmoid}(x)$	same
<i>Softplus</i>	Softplus function	$\text{softplus}(x)$	same
<i>Sum</i>	Sum of a vector	$\sum_{i=1}^D \mathbf{x}_i$	single ( $R^1$ )
<i>Mean</i>	Mean of a vector	$(\sum_{i=1}^D \mathbf{x}_i)/D$	single ( $R^1$ )
<i>FFN</i>	An FC layer mapping a vector to a scalar	$\mathbf{x}_i \times W_F, W_F \in R^{D \times 1}$	single ( $R^1$ )
<i>FFN_D</i>	An FC layer mapping a vector to a vector	$\mathbf{x}_i \times W_F, W_F \in R^{D \times D}$	constant ( $R^D$ )
<i>Add</i>	Addition	$x + y$	maximum
<i>Mul</i>	Multiplication	$x \cdot y$ or $x \odot y$	maximum
<i>Concat</i>	Concatenate and map two vectors	$[\mathbf{x}, \mathbf{y}] \times W_{Con}, W_{Con} \in R^{2 \times D \times D}$	constant ( $R^{1 \times D}$ )

'same' denotes the output shape is same as input  $x$ ;

'single' and 'constant' denote the output shapes are  $R^1$  and  $R^{1 \times D}$ ;

'maximum' denotes the maximal shape between  $x$  and  $y$ ;

many research domains [18] and made significant progress [17]. Existing NAS approaches have been used to search the best architectures of prevailing various DNNs, including convolution neural networks (CNNs) for computer vision (CV) tasks [29]–[31], recurrent neural networks (RNNs) for natural language processing (NLP) [22] and speech-related [23] tasks, graph neural networks (GNNs) for the tasks having non-Euclidean data [32], and Transformers for CV [33], NLP [34], and speech-related [35] tasks.

However, due to the difference in search space among different domains, these NAS approaches cannot be applied to search the optimal diagnostic function architecture. Besides, the architectures of existing diagnostic functions can be seen as a general model, which is used to handle three given types of inputs and output a scalar or a vector. To this end, this paper an evolutionary multi-objective optimization-based NAS approach for automatically designing effective diagnostic function architectures to build novel CDMs. Here, we first design an expressive search space by summarizing existing architectures, and then we propose MOGP to explore the devised search space by optimizing the objectives of model performance and model interpretability simultaneously. To the best of our knowledge, our work is the first to apply the NAS technique to the CD task.

### III. THE PROPOSED SEARCH SPACE FOR CD

As stated above, the search space of existing NAS approaches [18], [26], [32] is task-specific, which cannot be applied to CD for searching diagnostic functions.

To design the search space for CD, we first observe and summarize existing CD approaches that design novel diagnostic functions. Then we find that their diagnostic functions combine three types of input vectors in a linear or non-linear manner and finally output a scalar or a vector for the score prediction. In other words, the

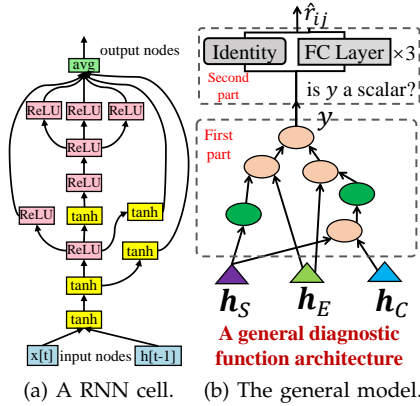


Fig. 2: Illustration of the proposed search space (the general diagnostic function architecture). The general model consists of two parts, and its first part (termed CD cell) holds at most three input nodes and several computation nodes (unary or binary).

diagnostic function architecture can be seen as a general model that has three input nodes, some internal nodes, and one output node. Both its output node and its internal nodes are computation nodes to handle their inputs by their adopted operators. We can find that the general model is similar to models under the search space of RNN in NAS [21], [36]. Fig. 2(a) plots the RNN cell found by *Efficient Neural Architecture Search* (ENAS) [36], where  $x[t]$  and  $h[t-1]$  are two input nodes,  $avg$  is the output node, and others are computation nodes.

By summarizing previous CD approaches, we collected some operators that be used for computation nodes of the general model. These operators are divided into two types, i.e., unary and binary operators, which are used to receive one input and two inputs, respectively. Here computation nodes (including the output node) in the general model can only handle at most two inputs, which is different from that of RNNs.

As a result, we take the general model as the proposed search space for CD, where 15 candidate operators in Table I can be adopted by each computation node and the following are their descriptions:

- **Unary operators.** Each unary operator only takes one input  $x$  and returns its output.  $FFN\_D$  returns the vectors,  $Sum$ ,  $Mean$ , and  $FFN$  return the scalar outputs, while the other eight unary operators return the outputs having the same shape as their inputs, which contains five arithmetic operators (i.e.,  $Neg$ ,  $Abs$ ,  $Inv$ ,  $Square$ , and  $Sqrt$ ) and three activation functions  $Tanh$  [37],  $Sigmoid$  [38], and  $Softplus$  [39].
- **Binary operators.** Three binary operators considered in the general model: in addition to addition  $Add$  and multiplication  $Mul$ , we further consider a  $Concat$  operator to aggregate two input vectors into one vector. Note that the output shapes of  $Add$  and  $Mul$  are determined by the maximal shape of two inputs. For example, when one input is a scalar  $x$  and another input is a vector  $\mathbf{y} \in R^{1 \times D}$ , the output shape is same as  $\mathbf{y}$  (equal to  $1 \times D$ ).

Here  $FFN$  and  $Concat$  are NN-based operators containing learnable parameters, which make the proposed search

space more expressive than that of RNN.

Note that the general model may output a scalar  $y$  or a vector  $\mathbf{y}$ , because the general model may adopt different operators while the output shapes of candidate operators are different. To make the prediction process successful, the general model has to execute the following process to get the prediction score of student  $s_i$  on exercise  $e_j$ :

$$\hat{r}_{ij} = \begin{cases} y, & \text{if } y \in R^1 \\ FC_3(FC_2(FC_1(\mathbf{y}))), & \text{if } \mathbf{y} \in R^{1 \times D} \end{cases}, \quad (3)$$

where  $FC_1(\cdot)$ ,  $FC_2(\cdot)$ , and  $FC_3(\cdot)$  are three FC layers with output dimensions  $H_1$ ,  $H_2$ , and  $H_3$ , respectively. The three FC layers are set to hold the monotonicity property according to the experiences in [11]. By doing so, the probability of a correct response to the exercise is monotonically increasing at any dimension of the student's knowledge proficiency, which enables FC layers to hold the same interpretability as the identity operation.

For better understanding, Fig. 2(b) presents the general diagnostic function architecture under the proposed search space. The general diagnostic function architecture (the general model) contains two parts. The first part (termed CD cell) is similar to the RNN cell in NAS, and the second part is a three-layer FC NN or an identity operation as shown in (3). The CD cell has several computation nodes (represented by ovals) and at most three input nodes ( $h_S$ ,  $h_E$ , and  $h_C$ , represented by triangles). Different from the RNN cell, its output node is also computation node, and computation nodes are selected from unary operators (denoted by green nodes) or binary operators (denoted by orange nodes). After obtaining the CD cell's output  $y$ , either the identity operation or the three-layer FC NN will be applied to get the final prediction  $\hat{r}_{ij}$ .

As stated in [18], [32], a promising search space should contain not only a large number of expressive neural architectures but also as many existing handcrafted architectures as possible. To demonstrate the effectiveness of the proposed search space, we take four representative CDMs, including IRT, MIRT, MF, and NCD, as illustrative examples. Fig. 4(a) to Fig. 4(d) present their diagnostic function architectures under the proposed search space. As can be seen, these typical CDMs can be easily represented under the proposed search space by specific computation nodes and selected input nodes.

#### IV. THE PROPOSED EMO-NAS-CD

This section will first present the proposed EMO-NAS-CD framework, and then sequentially give individual representation, objectives, and a tailored genetic operation. Finally, other details are introduced.

##### A. Overall Framework of EMO-NAS-CD

The main idea of the proposed EMO-NAS-CD is to search high-performance diagnostic function architectures holding high interpretability under the devised

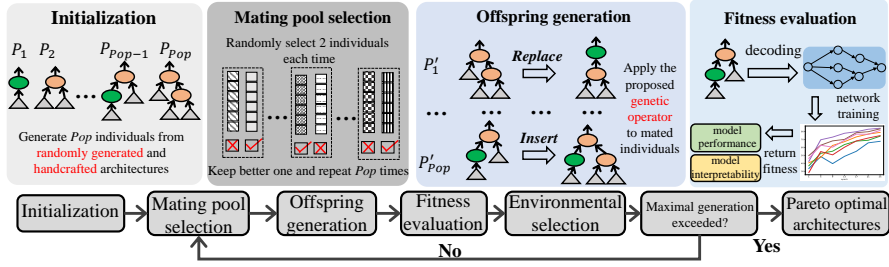


Fig. 3: **Bottom**: the overall framework of the proposed EMO-NAS-CD; **Upper**: illustrative examples of four components (population initialization, mating pool selection, offspring generation, and fitness evaluation).

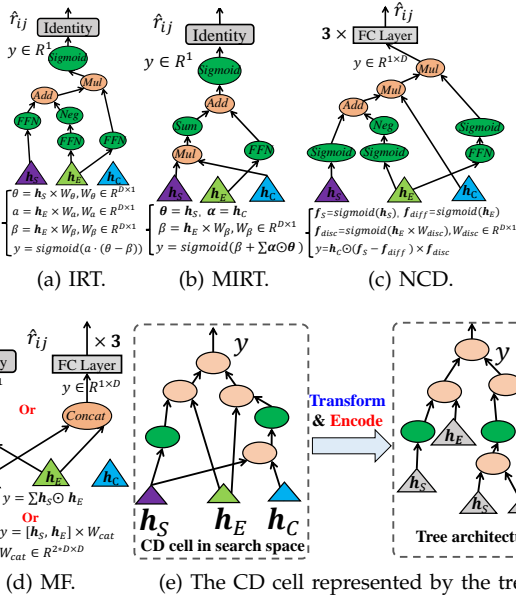


Fig. 4: (a), (b), (c) & (d): the diagnostic function architectures of four typical CDMs plotted under the proposed search space; (e): represent the CD cell of the general model by tree encoding.

search space. To this end, we aim to solve the NAS-CD task by optimizing a multi-objective optimization problem (MOP), which has two objectives: model performance and model interpretability. To avoid the difficulties of using vector-based encoding for the devised search space (e.g., variable-length encoding problem), we propose MOGP (a popular type of MOEAs [40]) to solve the MOP by transforming architectures into tree architectures and encoding them by trees, because genetic programming (GP) [41]–[43] can solve tree-encoding-based problems well. The devised MOGP follows the framework of NSGA-II [44], and we devise an effective genetic operation and a population initialization strategy for the MOGP. As can be seen that the proposed EMO-NAS-CD is a MOGP-based NAS approach for CD.

The overall framework of the proposed EMO-NAS-CD is summarized in Fig. 3, which is mainly composed of five steps. Firstly, a population initialization strategy (in Section IV-E1) is employed to randomly generate  $Pop$

### Algorithm 1: Main Steps of EMO-NAS-CD

- Input:**  $Gen$ : Maximum number of generations;  $Pop$ : Population size;  $Node_{range}$ : Range of the number of nodes in initialization;  
**Output:**  $P_{non}$ : Non-dominated individuals;
- 1:  $P \leftarrow Initialization(Pop, Node_{range})$ ;
  - 2: Evaluate each individual in  $P$  by training its corresponding architecture for  $Num_E$  epochs and obtain the objective values;
  - 3: **for**  $g = 1$  to  $Gen$  **do**
  - 4:  $P' \leftarrow Select\ Pop\ parent\ individuals\ from\ Population\ P$ ;  
 % Mating pool selection
  - 5:  $Q \leftarrow Genetic\ Operation(P')$ ; % Algorithm 2
  - 6: Evaluate each individual in  $Q$  by training its corresponding architecture for  $Num_E$  epochs and obtain the objective values;
  - 7:  $P \leftarrow Environment\ Selection(P \cup Q)$ ;
  - 8: **end for**
  - 9: Select non-dominated individuals  $P_{non}$  from  $P$  as the output
  - 10: **return**  $P_{non}$  ;

individuals as population  $P$ . Second, the standard binary tournament selection is employed to select individuals for getting the mating pool  $P'$ . Next, a novel genetic operation is applied to  $P'$  to generate offspring individuals and form the offspring population  $Q$ . Fourth, train the architecture of each individual of  $Q$  for a certain number of ( $Num_E$ ) epochs to compute its objective values. Fifth, the environmental selection in NSGA-II [44] will be employed to identify and maintain the individuals that hold better objective values from the union of population  $P$  and offspring population  $Q$ . The second to the fifth step will be repeated until the maximal number of generation  $Gen$  is exceeded, then the non-dominated individuals will finally be output. For details, Algorithm 1 also summarizes the main procedures of the proposed EMO-NAS-CD.

It is worth noting that there exist some individuals during the whole optimization process, whose neural architectures achieve terrible performance, nearly close to random performance. The reason behind this is that these architectures will encounter the gradient explosion problem when they continuously use some operations (e.g., *Square*, *Tanh*, and *Softplus*), which makes it difficult for general training paradigms to train them well. To solve this problem, in the individual evaluation, we adopt a simple early-stopping strategy [18] to stop the training of a neural architecture if its performance does not improve for several epochs.

### B. Individual Representation

To represent architectures in the proposed search space, vector-based encoding is naturally our first choice because of its high popularity in many real-world optimization problems. Suppose the vector-based encoding for  $i$ -th computation node of an architecture is  $n_i = \{link_1, link_2, Op\}$ , where  $link_1$  and  $link_2$  denote node  $n_i$  receiving which nodes' outputs and  $Op$  denotes which operator is adopted, and then each architecture is represented by a set of nodes  $\{n_i | 1 \leq i \leq num_c\}$  ( $num_c$  denotes the number of computation nodes).

However, as shown in Fig. 2(b), the architectures in the proposed search space are variable. Thus it is difficult and unsuitable to represent architectures by vector-based encoding due to two challenges. The first challenge is that  $num_c$  is not fixed but variable, and thus the vector-based encoding of each architecture is variable-length, which is difficult to solve by general MOEAs [26]. Secondly, different from the output node of the RNN cell, the output node in the proposed search space is a computation node and receives at most two inputs. This poses a decision constraint in using vector-based encoding as individual representation and thus is also difficult to solve.

To avoid the above issues, we propose to utilize tree-based representation to encode architectures in our proposed search space, and we propose MOGP to solve the MOP to search novel CDMs because of the superiority of GP in solving tree-encoding-based optimization problems [43]. For this aim, we have to transform the architectures under the proposed search space into their corresponding single-root tree architecture. Fig. 4 (e) gives the transform process by taking the general model as an illustrative example: the input nodes are seen as **the leaf nodes** of the tree architecture, the output node is equal to **the root node**, and the whole tree architecture can be seen as a single-root binary computation tree, where the obtained tree architecture is similar to the Koza-like tree in GP [45]. Based on the tree-based representation, the proposed MOGP can effectively search diagnostic function architectures but still needs the assistance of some tailored strategies, such as genetic operations and initialization strategies.

### C. Objectives

To make the searched architectures hold good performance and high interpretability, the proposed MOGP is to optimize the following MOP:

$$\max_{\mathcal{A}} F(\mathcal{A}) = \begin{cases} f_1(\mathcal{A}) = AUC(\mathcal{A}, D_{val}) \\ f_2(\mathcal{A}) = \text{model interpretability}(\mathcal{A}) \end{cases}, \quad (4)$$

where  $\mathcal{A}$  denotes the candidate architecture to be optimized.  $f_1(\mathcal{A})$  represents the AUC (*Area Under an ROC Curve*) value [46] of  $\mathcal{A}$  (i.e., model performance) on validation dataset  $D_{val}$ .  $f_2(\mathcal{A})$  represents the model interpretability of architecture  $\mathcal{A}$ , since an architecture holding high model interpretability is preferred for CD.

To obtain reasonable  $f_2(\mathcal{A})$ , an intuitive idea is to compute the model complexity by counting how many computation nodes and leaf nodes are in  $\mathcal{A}$ . But it is not reasonable [47] to some extent since much research [48] indicates that the model depth plays the most important role in the model interpretability. Besides, some research on interpretable trees [47], [49] further indicates that binary operators commonly provide better interpretability than unary operators. More importantly, recent CDMs prefer introducing extra inputs and more feature fusions in the models because it is easier to interpret the model performance [12], [16]. This implies that more inputs in CDMs represent higher interpretability, further indicating that binary operators are more important than unary ones since binary operators will introduce more inputs.

However, the model complexity that counts the number of nodes in  $\mathcal{A}$  can not reflect the above fact. As shown in Fig. 5, despite more nodes, we think  $\mathcal{A}_2$  holds better interpretability than  $\mathcal{A}_1$  due to a smaller depth. Due to larger breadth (more inputs),  $\mathcal{A}_4$  and  $\mathcal{A}_3$  should be better than  $\mathcal{A}_1$  but worse than  $\mathcal{A}_2$ .  $\mathcal{A}_5$  should be better than  $\mathcal{A}_3$  but worse than  $\mathcal{A}_4$  due to containing more nodes.

With the above considerations, we characterize the model interpretability of architecture  $\mathcal{A}$  by its tree's depth, breadth, and computation node number. The model interpretability of  $\mathcal{A}$  is first determined by the tree depth  $depth$ , then by the tree breadth  $breadth$  (equal to the number of leaf nodes), and finally by the number of computation nodes  $num_c$ . As a consequence, the  $f_2(\mathcal{A})$  can be computed by

$$f_2(\mathcal{A}) = \left(1 - \frac{depth - 1}{10}\right) + \frac{breadth}{200} + \left(0.001 - \frac{num_c}{20000}\right), \quad (5)$$

where we make the depths of all architectures less than 10 in this paper to hold high model interpretability and thus  $f_2(\mathcal{A}) \in (0, 1)$  has five decimal places. The first decimal place is determined by  $depth$ , The second and third decimal places are determined by  $breadth$ , and the remaining decimal places are determined by  $num_c$ . Note that three parameters (10, 200, 2000) are empirically set and can be other choices, which will not affect the proposed approach's result as long as two criteria are met. Firstly, the decimal place(s) determined by  $depth$ ,  $breadth$ , and  $num_c$  do not affect each other; secondly, the decimal place(s) determined by  $depth$  is most important, followed by  $breadth$ , and finally  $num_c$ .

In Fig. 5, the depths of five architectures are 3, 2, 3, 3, and 3, their breadths are 1, 2, 3, 4, and 4, and their computation node numbers are 3, 3, 4, 4, and 5. According to (5), their second objective values are 0.80585, 0.91085, 0.81580, 0.82080, and 0.82075, respectively, which are consistent with our consideration.

### D. Genetic Operation

For effective offspring generation in the proposed MOGP, we propose an effective genetic operation based on four sub-genetic operations that modified and inspired from GP [41]–[43].

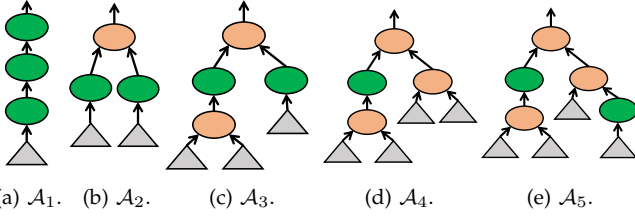


Fig. 5: An illustration of the model interpretability objective by five diagnostic function architectures including  $\mathcal{A}_1$ ,  $\mathcal{A}_2$ ,  $\mathcal{A}_3$ ,  $\mathcal{A}_4$ , and  $\mathcal{A}_5$ .

The following introduces four modified sub-genetic operations: *Exchange*, *Delete*, *Replace*, and *Insert*.

- *Exchange*. Given two individuals,  $\mathbf{P}'_1$  and  $\mathbf{P}'_2$ , randomly select two sub-trees,  $t_1$  and  $t_2$ , from the trees corresponding to two individuals, respectively, and then exchange two sub-trees to generate two new trees and form two offspring individuals,  $\mathbf{O}_1$  and  $\mathbf{O}_2$ . (The root nodes will not be selected.)
- *Delete*. Given a parent individual  $\mathbf{P}'_1$ , randomly select a computation node from the tree corresponding to  $\mathbf{P}'_1$ . To delete this node, one of the left and right child trees of this node will be randomly connected to its parent node (if exists). The newly generated tree can form the offspring individual  $\mathbf{O}_1$ .
- *Replace*. For the tree corresponding to individual  $\mathbf{P}'_1$ , randomly select a node to be replaced and replace the node's operator by a new operator randomly sampled from Table I. If the original operator is unary but the sampled operator is binary, a new leaf node will be generated and connected to this node as its child tree, where the new leaf node is randomly sampled from  $\{h_S, h_E, h_C\}$ . If the original operator is binary but the sampled operator is unary, only one of the left and right child trees of this node will be kept. As a result, offspring individual  $\mathbf{O}_1$  can be obtained based on the revised tree.
- *Insert*. A new operator is first randomly sampled from the predefined operators, and a computation node is randomly selected from individual  $\mathbf{P}'_1$ . Then, the sampled operator is inserted between this node and its parent node (if exists) as a new computation node. If the sampled operator is binary, an additional leaf node will be randomly sampled from  $\{h_S, h_E, h_C\}$  and added to the new computation node as its child tree. Finally, offspring individual  $\mathbf{O}_1$  will be generated.

Note that the root node will not be involved in *Exchange* since the *Exchange* operation will be meaningless or ineffective if root nodes are selected. For a better understanding of the above operations, Fig. 6 gives some illustrative examples of generating offspring individuals. The pink area denotes the selected computation nodes (or corresponding sub-trees) needed to be handled, and the light purple area represents the executed changes.

As can be seen, *Exchange* will lead to big modifications between generated individuals and corresponding parent individuals, while other operations commonly lead to small modifications. Therefore, the *Exchange* operation can be used for exploration, and others can be used for exploitation [50]. Equipped with four sub-genetic operations, we empirically combine them to form our proposed genetic operation, whose basic procedures are

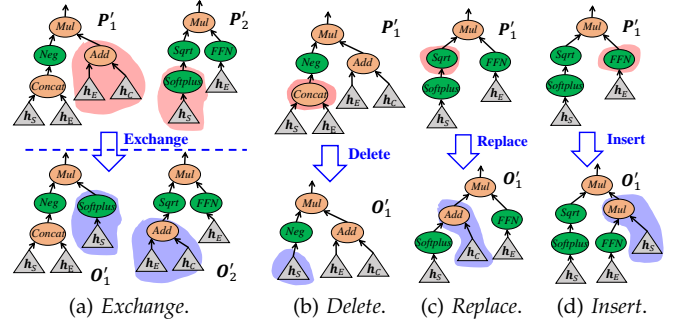


Fig. 6: Illustrative examples of four sub-genetic operations, where the second parts are not plotted.

summarized in Algorithm 2. Four operations are called four sub-genetic operations because they can constitute many other genetic operations when adopting different combination manners. In Algorithm 2, two individuals  $\mathbf{P}'_i$  ( $i$ -th individual in  $\mathbf{P}'$ ) and  $\mathbf{P}'_{i+1}$  are first selected from the mating pool  $\mathbf{P}'$ , and the numbers of computation nodes in the two individuals are computed as  $num_c^i$  and  $num_c^{i+1}$  (Lines 3-4). Second, randomly sample an integer  $rand$  from  $\{1, 2, 3, 4\}$  if both  $num_c^i$  and  $num_c^{i+1}$  are not smaller than 2, otherwise randomly sample  $rand$  from  $\{3, 4\}$ . Numbers 1, 2, 3, and 4 correspond to *Exchange*, *Delete*, *Replace*, and *Insert*, respectively (Lines 5-9). This is because *Exchange* and *Delete* will be ineffective, even meaningless, if there is only one computation node in the individual. Third, the sub-genetic operation corresponding to  $rand$  will be applied to  $\mathbf{P}'_i$  and  $\mathbf{P}'_{i+1}$  to generate offspring individuals  $\mathbf{O}_1$  and  $\mathbf{O}_2$  (Lines 10-14). Next, the obtained  $\mathbf{O}_1$  and  $\mathbf{O}_2$  will be added to the offspring population  $Off$  (Line 15). The first to the fourth step will be repeated until all offspring individuals are generated. After that, an individual repair strategy in Section IV-E2 is used to make offspring individuals feasible since there exist some constraints for some operators in computation nodes of trees (Line 17). For example, *Sum*, *Mean*, *FFN*, and *Concat* only receive vectors as their inputs. Finally, the obtained offspring population  $Off$  is output.

### E. Related Details

In the mating pool selection of EMO-NAS-CD, two individuals are first randomly selected each time, and then their non-dominated front sizes and crowding distance values are compared to keep the better one. The computation of non-dominated front size and crowding distance for each individual is the same as for NSGA-II [44]. Due to the simple topologies of tree architectures, this will generate many duplicated individuals. To address this issue, a simple archive stores the individuals that have appeared and identifies whether a newly generated individual has already occurred. In addition, there are the population initialization strategy and the individual repairing strategy in the proposed approach.

**Algorithm 2: Genetic Operation**


---

**Input:**  $\mathbf{P}'$ : Mating pool,  $Pop$ : Population size  
**Output:**  $Off$ : Offspring ;

```

1:  $Off \leftarrow \emptyset$ ;
2: for  $i = 1$  to  $Pop$  do
3:    $\mathbf{P}'_i, \mathbf{P}'_{i+1} \leftarrow$  Sequentially select two individuals from  $\mathbf{P}'$ ;
4:    $num_c^i, num_c^{i+1} \leftarrow$  Get the numbers of computation nodes in  $\mathbf{P}'_i$  and  $\mathbf{P}'_{i+1}$ ;
5:   if  $num_c^i \geq 2$  and  $num_c^{i+1} \geq 2$  then
6:      $rand \leftarrow$  Randomly sample an integer from  $\{1, 2, 3, 4\}$ ;
7:   else
8:      $rand \leftarrow$  Randomly sample an integer from  $\{3, 4\}$ ;
9:   end if
10:  if  $rand = 1$  then
11:     $\mathbf{O}_1, \mathbf{O}_2 \leftarrow$  Apply Exchange to  $\mathbf{P}'_i$  and  $\mathbf{P}'_{i+1}$ ;
12:  else if  $rand = 2/3/4$  then
13:     $\mathbf{O}_1, \mathbf{O}_2 \leftarrow$  Apply Delete/Replace/Insert to  $\mathbf{P}'_i$  and  $\mathbf{P}'_{i+1}$ ;
14:  end if
15:   $Off \leftarrow Off \cup \mathbf{O}_1 \cup \mathbf{O}_2, i \leftarrow i + 2$ ;
16: end for
17: Individual repairing for  $Off$ ; % Section IV-E2
18: return  $Off$ ;

```

---

1) *Population Initialization*: Instead of evolving architectures entirely from scratch [17], [26], we aim to introduce prior knowledge about existing CDMs' diagnostic functions into the search process.

To this end, one half of the individuals in the population are generated from four existing CDMs (IRT, MIRT, MF, and NCD) by applying the proposed genetic operation. To maintain the diversity of the population and avoid getting trapped into local optima, another half of individuals are randomly generated from scratch. Here, we utilize a hyperparameter  $Node_{range} = \{node_{h1}, node_{h2}\}$  to limit the computation node number sampled in each randomly generated individual. Here  $node_{h1}$  and  $node_{h2}$  refer to the lower and upper bounds of the number of generated nodes.

2) *Individual Repair*: Most operators in Table I can be applied to the input with any shape, except for *Sum*, *Mean*, *FFN*, and *Concat*, which can only receive one-dimensional vectors as their inputs. The first three operators are specially used to extract a high-level scalar feature from vectors, while *Concat* is specially used to concatenate and map two vectors to one vector.

Therefore, one generated individual is infeasible and needs repairing if its contained nodes are equipped with the above four operators but take scalar inputs (termed infeasible nodes). To tackle this issue, we first execute the post-order traversal for each individual to check whether each node is feasible and then directly replace the operator of the infeasible node with other unary operators or other binary operators (e.g, replace *Concat* by *Add*, and replace *Mean* by *Neg*).

3) *Complexity Analysis*: The time complexity of the proposed EMO-NAS-CD is mainly determined by two components, i.e., the training of each architecture and the optimization process of NSGA-II. Suppose the size of a training dataset is  $|D_{train}|$ , the time complexity of training each architecture [51] is  $O(Num_E \times |D_{train}| \times D)$ , and the time complexity of one generation of NSGA-II is

TABLE II: Statistics of two popular education datasets.

Dataset	ASSISTments [52] <sup>①</sup>	SLP [53] <sup>②</sup>
# Students	4,163	1,499
# Concepts	123	34
# Exercises	17,746	907
# Response logs	324,572	57,244

$O(Pop^2)$  [44]. Therefore, the overall time complexity of EMO-NAS-CD is  $O(Pop \times Gen \times Num_E \times |D_{train}| \times D) + O(Pop^2 \times Gen)$ . Since  $Num_E \times |D_{train}| \times D \gg Pop \times Gen$ , the time complexity of EMO-NAS-CD can be regarded as  $O(Pop \times Gen \times Num_E \times |D_{train}| \times D)$ .

On the other hand, its space complexity is mainly determined by the population and the offspring population, and each population has  $Pop$  individuals encoded by trees. Suppose the average number of computation nodes in the trees is  $AvgNum$ , the space complexity of an individual is  $O(AvgNum * 3)$  since each node needs three numbers to specify its operation and two subtrees. As a result, the whole space complexity of EMO-NAS-CD is  $O(AvgNum * 3 \times Pop \times 2)$ , i.e.,  $O(AvgNum \times Pop \times 6)$ .

## V. EXPERIMENTS

## A. Experimental Settings

1) *Datasets*: To verify the effectiveness of the proposed EMO-NAS-CD, we conducted experiments on two real-world education datasets, including ASSISTments [52] and SLP [53]. We have summarized the statistics of two datasets in Table II and presented the descriptions of two datasets as follows:

- **ASSISTments** (*ASSISTments 2009-2010 skill builder*) [52] is an openly available dataset created in 2009 by the ASSISTments online tutoring service system. Here we adopted the public corrected version that does not contain duplicate data. As can be seen, there are more than 4 thousand students, nearly 18 thousand exercises, and over 300 thousand response logs in the dataset.
- **SLP** (*Smart Learning Partner*) [53] is another public education dataset published in 2021. SLP collects the regularly captured academic performance data of learners during their three-year study on eight different subjects, including Chinese, mathematics, English, physics, chemistry, biology, history and geography. The dataset contains nearly 58 thousand response logs of 1,499 students on 907 exercises.

According to the experiences of previous work [11], [13], [14], we filtered out students with less than 15 response logs for all datasets to ensure that there are sufficient data to model each student for diagnosis.

2) *Compared Approaches and Metrics*: To validate the effectiveness of the proposed approach, we compared the diagnostic function architectures found by the proposed EMO-NAS-CD with state-of-the-art CDMs, including DINA [7], IRT [6], and MIRT [8], MF [9], NCD [11], RCD [13], CDGK [14], and KSCD [16]. The detailed descriptions of these comparison CDMs can be found in Section II-B. The source codes of most compared approaches are available at <https://github.com/orgs/bigdata-ustc/repositories>. Note that the results of RCD on SLP are not reported since RCD needs extra manually enhanced inputs that SLP does not have.

TABLE III: The prediction performance comparison between the architectures found by the proposed EMO-NAS-CD (one run) and comparison CDMs in terms of ACC, RMSE, and AUC values (averaged on 30 runs), obtained on the test datasets of ASSISTments and SLP. Best results in each column (excluding  $\overline{A1-A7}$  and  $\overline{S1-S7}$ ) are highlighted.

Train/test ratio		50%/50%			60%/40%			70%/30%			80%/20%		
Dataset	Method	ACC	RMSE	AUC									
ASSISTments	DINA	0.6532	0.4821	0.7103	0.6617	0.4771	0.7206	0.6672	0.4735	0.7260	0.6747	0.4699	0.7341
	IRT	0.6944	0.4595	0.7102	0.7006	0.4545	0.7203	0.7024	0.4536	0.7241	0.7058	0.4511	0.7285
	MIRT	0.6885	0.5309	0.7141	0.6945	0.5283	0.7203	0.7069	0.5152	0.7412	0.7251	0.5005	0.7599
	MF	0.6920	0.4577	0.7227	0.6927	0.4553	0.7242	0.6936	0.4542	0.7280	0.6930	0.4551	0.7244
	NCD	0.7155	0.4411	0.7396	0.7208	0.4380	0.7480	0.7243	0.4344	0.7548	0.7279	0.4321	0.7523
	RCD	0.7281	0.4255	0.7618	0.7288	0.4244	0.7612	0.7307	0.4257	0.7655	0.7357	0.4210	0.7728
	CDGK	0.7121	0.4398	0.7360	0.7192	0.4344	0.7454	0.7226	0.4338	0.7506	0.7342	0.4251	0.7567
	KSCD	0.7167	0.4245	0.7470	0.7205	0.4239	0.7534	0.7249	0.4179	0.7594	0.7351	0.4140	0.7636
	$\overline{A1}$	0.7101	0.4423	0.7410	0.7236	0.4367	0.7495	0.7246	0.4335	0.7528	0.7276	0.4301	0.7621
	( $\overline{A1}$ )	0.7126	0.4417	0.7414	0.7218	0.4369	0.7491	0.7260	0.4277	0.7549	0.7289	0.4319	0.7644
	$\overline{A2}$	0.7165	0.4336	0.7545	0.7238	0.4301	0.7610	0.7263	0.4287	0.7629	0.7452	0.4272	0.7726
	( $\overline{A2}$ )	0.7145	0.4375	0.7549	0.7226	0.4313	0.7593	0.7276	0.4263	0.7655	0.7449	0.4268	0.7731
	$\overline{A3}$	0.7229	0.4328	0.7562	0.7305	0.4265	0.7647	0.7315	0.4263	0.7682	0.7353	0.4252	0.7766
	( $\overline{A3}$ )	0.7237	0.4300	0.7567	0.7312	0.4285	0.7658	0.7307	0.4281	0.7688	0.7353	0.4241	0.7763
	$\overline{A4}$	0.7415	0.4350	0.7602	0.7560	0.4238	0.7812	0.7674	0.4152	0.7965	0.7857	0.4001	0.8210
	( $\overline{A4}$ )	0.7406	0.4339	0.7608	0.7561	0.4220	0.7809	0.7662	0.4173	0.7945	0.7862	0.3995	0.8211
	$\overline{A5}$	0.7377	0.4397	0.7814	0.7530	0.4317	0.8019	0.7630	0.4215	0.8182	0.7810	0.4107	0.8409
( $\overline{A5}$ )	0.7388	0.4409	0.7825	0.7536	0.4331	0.8014	0.7634	0.4206	0.8174	0.7817	0.4123	0.8414	
$\overline{A6}$	0.7441	0.4355	0.7860	0.7593	0.4252	0.8066	0.7712	0.4183	0.8244	0.7884	0.4018	0.8474	
( $\overline{A6}$ )	0.7442	0.4364	0.7857	0.7585	0.4264	0.8045	0.7725	0.4207	0.8255	0.7880	0.4003	0.8477	
$\overline{A7}$	0.7438	0.4372	0.7839	0.7609	0.4237	0.8071	0.7735	0.4148	0.8250	0.7916	0.3993	0.8496	
( $\overline{A7}$ )	0.7441	0.4369	0.7847	0.7614	0.4248	0.8073	0.7727	0.4130	0.8250	0.7915	0.3996	0.8499	
SLP	DINA	0.6026	0.5200	0.6444	0.5735	0.5348	0.6240	0.6201	0.5063	0.6695	0.5871	0.5220	0.6565
	IRT	0.6048	0.4960	0.7061	0.6381	0.4779	0.7351	0.6502	0.4711	0.7340	0.6882	0.4540	0.7712
	MIRT	0.7145	0.4948	0.7595	0.7246	0.4842	0.7750	0.7376	0.4757	0.7852	0.7364	0.4772	0.7847
	MF	0.6655	0.4199	0.8229	0.7807	0.4081	0.8358	0.7243	0.4036	0.8372	0.7876	0.3997	0.8428
	NCD	0.7550	0.4425	0.8137	0.7741	0.4262	0.8330	0.7703	0.4246	0.8326	0.7880	0.4012	0.8397
	RCD	0.7544	0.4429	0.8130	0.7755	0.4244	0.8334	0.7716	0.4257	0.8313	0.7879	0.3844	0.8421
	CDGK	0.7544	0.4429	0.8130	0.7755	0.4244	0.8334	0.7716	0.4257	0.8313	0.7879	0.3844	0.8421
	KSCD	0.7563	0.4258	0.8218	0.7738	0.4125	0.8391	0.7710	0.4085	0.8377	0.7857	0.3844	0.8464
	$\overline{S1}$	0.7674	0.4279	0.8224	0.7746	0.4183	0.8321	0.7756	0.4210	0.8345	0.7872	0.4093	0.8439
	( $\overline{S1}$ )	0.7677	0.4286	0.8230	0.7739	0.4166	0.8320	0.7737	0.4214	0.8336	0.7883	0.4085	0.8446
	$\overline{S2}$	0.7741	0.4219	0.8246	0.7840	0.4051	0.8441	0.7856	0.3942	0.8497	0.7915	0.3912	0.8560
	( $\overline{S2}$ )	0.7731	0.4218	0.8237	0.7843	0.4034	0.8448	0.7868	0.3939	0.8510	0.7921	0.3922	0.8563
	$\overline{S3}$	0.7722	0.4215	0.8349	0.7735	0.4110	0.8457	0.7772	0.3997	0.8534	0.7855	0.3912	0.8572
	( $\overline{S3}$ )	0.7733	0.4206	0.8359	0.7743	0.4112	0.8444	0.7769	0.4000	0.8524	0.7855	0.3913	0.8577
	$\overline{S4}$	0.7806	0.3933	0.8429	0.7916	0.3871	0.8539	0.7861	0.3904	0.8554	0.7964	0.3797	0.8635
	( $\overline{S4}$ )	0.7812	0.3928	0.8441	0.7900	0.3891	0.8522	0.7883	0.3895	0.8566	0.7966	0.3799	0.8637
	$\overline{S5}$	0.7789	0.3934	0.8439	0.7933	0.3840	0.8561	0.7832	0.3863	0.8559	0.7962	0.3794	0.8641
( $\overline{S5}$ )	0.7786	0.3949	0.8433	0.7930	0.3847	0.8566	0.7831	0.3860	0.8555	0.7949	0.3813	0.8642	
$\overline{S6}$	0.7802	0.3930	0.8470	0.7955	0.3844	0.8579	0.7828	0.3877	0.8580	0.8001	0.3773	0.8669	
( $\overline{S6}$ )	0.7803	0.3927	0.8475	0.7953	0.3844	0.8581	0.7810	0.3888	0.8567	0.7987	0.3779	0.8663	
$\overline{S7}$	0.7786	0.3973	0.8446	0.7941	0.3865	0.8587	0.7854	0.3833	0.8621	0.8023	0.3781	0.8685	
( $\overline{S7}$ )	0.7779	0.4002	0.8435	0.7945	0.3866	0.8577	0.7841	0.3844	0.8622	0.8031	0.3796	0.8683	

To measure the performance obtained by all CDMs, three evaluation metrics including AUC, accuracy (ACC), and root mean square error (RMSE) are adopted.

### 3) Parameter Settings:

- **1. Architecture Settings** The dimension  $D$  is equal to the number of knowledge concepts  $K$ ,  $H_1$ ,  $H_2$ , and  $H_3$  are set to 512, 256, and 1, respectively.
- **2. Search Settings** During the search process in the proposed EMO-NAS-CD, each student's response logs in each dataset are randomly split into 70%, 10%, and 20% as training, validating, and testing datasets, respectively. To train the architecture encoded by each individual, the *Adam* optimizer with a learning rate of 0.001 is used to optimize the Cross-Entropy loss between the prediction results and the targets, where the size of each batch is set to 128, and the number of training epochs  $Num_E$  is set to 30. For the proposed EMO-NAS-CD, the population size  $Pop$  is set to 100, the maximal number of generation  $Gen$  is set to 100, and the initial node range  $Node_{range}$  is set to  $\{2, 4\}$ .
- **3. Training Settings** For more convincing results, we adopted multiple different settings to split the dataset into training and test datasets for evaluating the model performance, where the settings contain 50%/50%, 60%/40%, 70%/30%, and 80%/20% as suggested in [13]. Each found architecture needs to be retrained from scratch for 50 epochs, the settings are the same as that in the above search settings. For a fair comparison, the parameter settings of all comparison CDMs are the same as those in their original papers to hold their best performance.

All experiments were conducted on a NVIDIA RTX

3090 GPU. Our source code can be available at <https://github.com/DevilYangS/EMO-NAS-CD>.

### B. Effectiveness of The Proposed EMO-NAS-CD

Table III summarizes the prediction performance comparison between the proposed EMO-NAS-CD and comparison CDMs in terms of ACC, RMSE, and AUC values that are averaged on 30 independent runs on the two datasets, where five different splitting settings are considered. Here seven architectures (with different degrees of model interpretability) found by EMO-NAS-CD in a single run are selected for comparison, where architectures  $A1$  to  $A7$  are found on the ASSISTments and architectures  $S1$  to  $S7$  are found on the SLP. To this end, for some architectures that have similar model interpretability, the architecture with the best performance among these architectures will be selected for final comparison. For more convincing explanations, Table III further shows the results of  $\overline{A1}$  ( $\overline{S1}$ ) to  $\overline{A7}$  ( $\overline{S7}$ ).  $\overline{A1}$  refers to the average results on ten different runs of EMO-NAS-CD. In each run, the architecture that has similar interpretability to  $A1$  is used to compute  $\overline{A1}$ , which is

TABLE IV: Friedman test with Nemenyi post-hoc procedure on the results of Table III. Architectures  $\overline{A1}$  to  $\overline{A7}$  are denoted by ① to ⑦,  $\overline{S1}$  to  $\overline{S7}$  are denoted by ① to ⑦, DINA, IRT, MIRT, MF, NCD, RCD, CDGK, and KSCD are denoted by  $\mathcal{D}$ ,  $\mathcal{I}$ ,  $\mathcal{M}$ ,  $\mathcal{F}$ ,  $\mathcal{N}$ ,  $\mathcal{R}$ ,  $\mathcal{C}$ , and  $\mathcal{K}$ , respectively. Here left and right tables summarize the analysis results on the ASSISTments and SLP, respectively, where ‘1’ indicates significant difference and ‘0’ otherwise.

Friedman Test with Nemenyi Post-hoc on the ASSISTments																
Method	⑦	⑥	④	⑤	$\mathcal{R}$	③	$\mathcal{K}$	①	①	$\mathcal{N}$	$\mathcal{C}$	$\mathcal{I}$	$\mathcal{F}$	$\mathcal{M}$	$\mathcal{D}$	Rank
⑦	-	0	0	0	0	0	0	0	1	1	1	1	1	1	1	2.08
⑥	0	-	0	0	0	0	0	0	1	1	1	1	1	1	1	2.67
④	0	0	-	0	0	0	0	0	1	1	1	1	1	1	1	3.17
⑤	0	0	0	-	0	0	0	0	0	0	1	1	1	1	1	4.50
$\mathcal{R}$	0	0	0	0	-	0	0	0	0	0	1	1	1	1	1	5.33
③	0	0	0	0	0	-	0	0	0	0	1	1	1	1	1	5.88
$\mathcal{K}$	0	0	0	0	0	0	-	0	0	0	1	1	1	1	1	6.50
②	0	0	0	0	0	0	0	-	0	0	0	1	1	1	1	6.54
①	1	1	0	0	0	0	0	0	-	0	0	0	0	0	0	9.17
$\mathcal{N}$	1	1	1	0	0	0	0	0	0	-	0	0	0	0	0	10.17
$\mathcal{C}$	1	1	1	0	0	0	0	0	0	0	-	0	0	0	0	10.17
$\mathcal{I}$	1	1	1	1	1	1	1	0	0	0	0	-	0	0	0	13.13
$\mathcal{F}$	1	1	1	1	1	1	1	1	0	0	0	0	-	0	0	13.17
$\mathcal{M}$	1	1	1	1	1	1	1	1	0	0	0	0	0	-	0	13.38
$\mathcal{D}$	1	1	1	1	1	1	1	1	0	0	0	0	0	0	-	14.17
$p$ -values		2.29e-24					Significance level $\alpha$ 0.05									

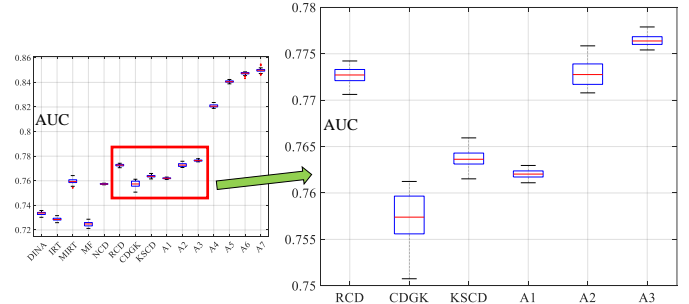
  

Friedman Test with Nemenyi Post-hoc on the SLP															
Method	⑦	⑦	④	⑤	②	③	$\mathcal{F}$	$\mathcal{K}$	①	$\mathcal{C}$	$\mathcal{N}$	$\mathcal{M}$	$\mathcal{I}$	$\mathcal{D}$	Rank
⑦	-	0	0	0	0	0	0	0	1	1	1	1	1	1	1.83
⑦	0	-	0	0	0	0	0	0	1	1	1	1	1	1	2.25
④	0	0	-	0	0	0	0	0	1	1	1	1	1	1	2.92
⑤	0	0	0	-	0	0	0	0	0	1	1	1	1	1	3.25
②	0	0	0	0	-	0	0	0	0	0	1	1	1	1	5.42
③	0	0	0	0	0	-	0	0	0	0	0	1	1	1	6.25
$\mathcal{F}$	0	0	0	0	0	0	-	0	0	0	0	0	0	1	7.42
$\mathcal{K}$	1	1	0	0	0	0	0	-	0	0	0	0	0	0	8.17
①	1	1	1	0	0	0	0	0	-	0	0	0	0	0	8.67
$\mathcal{C}$	1	1	1	1	0	0	0	0	0	-	0	0	0	0	9.58
$\mathcal{N}$	1	1	1	1	0	0	0	0	0	0	-	0	0	0	10.25
$\mathcal{M}$	1	1	1	1	1	0	0	0	0	0	0	-	0	0	12.25
$\mathcal{I}$	1	1	1	1	1	1	0	0	0	0	0	0	-	0	12.75
$\mathcal{D}$	1	1	1	1	1	1	1	0	0	0	0	0	0	-	14.00
$p$ -values		2.62e-24					Significance level $\alpha$ 0.05								

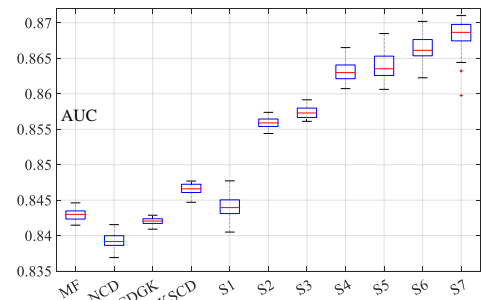
the same to obtain  $\overline{A2}$  to  $\overline{A7}$  and  $\overline{S1}$  to  $\overline{S7}$ . Besides, the Friedman test with Nemenyi procedure [54] (under significance level  $\alpha=0.05$ ) was conducted on the results of comparison CDMs and  $\overline{A1}$  ( $\overline{S1}$ ) to  $\overline{A7}$  ( $\overline{S7}$ ), which is a nonparametric statistical procedure to check whether a set of samples are statistically different. Table IV summarizes the statistical results including significance analysis and rank of each method, where ‘1’ indicates significant difference between two methods and ‘0’ otherwise.

As can be observed from Table III and Table IV, nearly all architectures found by EMO-NAS-CD (except for the simplest architectures  $A1$  and  $S1$ ) exhibit significantly better performance than all comparison CDMs. Take the results under the splitting setting of 80%/20% for analysis, and the boxplots for AUC values (under this setting) of comparison CDMs and seven found architectures are further presented in Fig.7 for explicit observation. As can be seen, the most effective architecture  $A7$  outperforms the current best CDM (RCD) by over 0.07 on the ASSISTments dataset in terms of the AUC value. Even for the simplest architecture  $A1$ , there still holds the superiority of performance over most CDMs, which is competitive to KSCD and only worse than RCD, but KSCD and RCD use extra input information to enhance the performance. Therefore, compared to the CDMs that do not have such input information, the performance difference between our best-found architectures and these CDMs is more significant: the performance leading of  $A7$  over the best of these CDMs is up to 0.08 in terms of AUC values, and architecture  $A1$  also outperforms these CDMs. It can be seen that the proposed approach achieves such a tremendous performance improvement by only designing more effective architectures without extra input information. In addition, we can find that the standard deviation of the proposed approach is very small from the comparisons between  $A1$  to  $A7$  and  $\overline{A1}$  to  $\overline{A7}$ . We can make the same observations and conclusions based on the results on the SLP dataset.

For a deep insight into found architectures, we pre-



(a) Boxplot on the ASSISTments.



(b) Boxplot on the SLP (excluding DINA, IRT, and MIRT due to their poor performance).

Fig. 7: Boxplots for AUC values (under the ratio of 80%/20%) of comparison CDMs and seven found architectures on both datasets.

sented all non-dominated individuals found by the proposed approach on two datasets in Fig. 8 and Fig. 9, where the architectures corresponding to these individuals are further plotted in the right parts of two figures. As can be observed,  $A1$  or  $S1$  is the shallowest architecture, which holds the highest model interpretability but worse prediction performance, while  $A7$  or  $S7$  is the deepest architecture, which holds the best performance but the worst interpretability among all selected architectures.

In addition, we can obtain some interesting and insightful observations from these best-found architectures

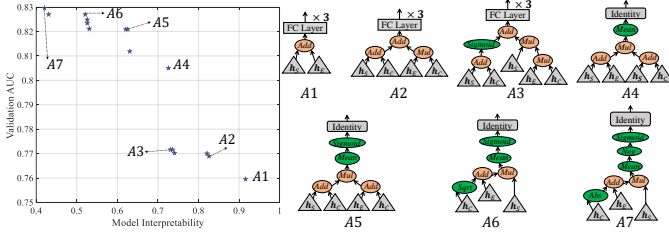


Fig. 8: The non-dominated individuals found by the proposed EMO-NAS-CD on the ASSISTments and the visualization of architecture A1 to architecture A7.

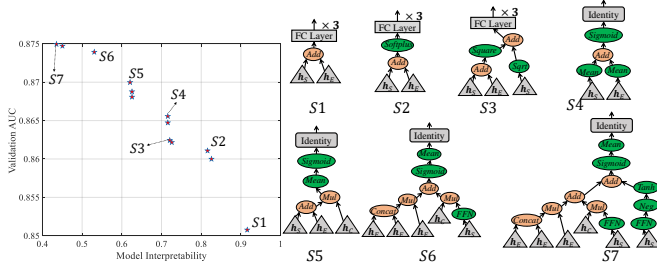


Fig. 9: The non-dominated individuals found by the proposed EMO-NAS-CD on the SLP and the visualization of architecture S1 to architecture S7.

on two datasets. Firstly, from the comparisons of S1 and S2, A2 and A3, as well as A4 and A5, we can find that adding a proper activation such as *Sigmoid* and *Softplus* can enhance the model performance without losing interpretability; Secondly, in most shallower architectures, the exercise-related input  $h_E$  tends to be directly combined with the student-related input  $h_S$  by some binary operators, while in most deeper architectures,  $h_E$  tends to be first combined with the knowledge concept-related input  $h_C$  and then combined with  $h_S$ . Finally, all shallower architectures prefer FC layers as their second parts to output the final prediction, while for the deeper architectures with better performance, the *Identity* operation seems to be a more effective second part. These deeper architectures commonly obtain the final prediction with the assistance of the *Mean* operator. The above observations provide some valuable guidelines for manually designing novel CDMs.

### C. Architecture Transferring Validation

As can be seen from Figs. 8 and 9, the two sets of selected best-architectures on two datasets are a bit different from each other. Only architecture A1 is same as architecture S1 and similar to S2 and S4, and architectures A6 and A7 are similar to architecture S5.

To further investigate the transferability and generalization of the found architectures, Table V presents the performance of architectures A2 to A7 and architectures S2 to S7 on the two datasets under the splitting setting of 80%/20%, where the results of A1 and S1 are not

TABLE V: The performance comparison between the architectures found by EMO-NAS-CD on the ASSISTments and the architectures found by EMO-NAS-CD on the SLP. The best results in each column are highlighted. Results are obtained on test datasets.

Methods	ASSISTments			SLP		
	ACC $\uparrow$	RMSE $\downarrow$	AUC $\uparrow$	ACC $\uparrow$	RMSE $\downarrow$	AUC $\uparrow$
A2	0.7452	0.4272	0.7726	0.7865	0.4030	0.8415
A3	0.7353	0.4252	0.7766	0.7867	0.4001	0.8365
A4	0.7857	0.4001	0.8210	0.7718	0.4105	0.8385
A5	0.7810	0.4107	0.8409	0.7777	0.3924	0.8525
A6	0.7884	0.4018	0.8474	0.7671	0.3966	0.8445
A7	<b>0.7916</b>	<b>0.3993</b>	<b>0.8496</b>	0.7722	0.4007	0.8356
S2	0.7512	0.4788	0.7880	0.7915	0.3912	0.8560
S3	0.7435	0.4942	0.7786	0.7855	0.3912	0.8572
S4	0.7310	0.4218	0.7706	0.7964	0.3797	0.8635
S5	0.7355	0.4233	0.7736	0.7962	0.3794	0.8641
S6	0.7338	0.4281	0.7781	0.8001	<b>0.3773</b>	0.8669
S7	0.7321	0.4274	0.7769	<b>0.8023</b>	0.3781	<b>0.8685</b>

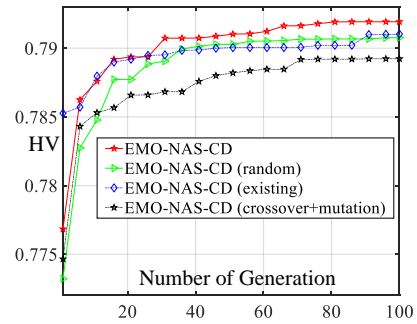


Fig. 10: Convergence profiles of HV obtained by EMO-NAS-CD and its variants on the SLP dataset.

contained since they have the same architecture. As can be observed, the architectures found on the ASSISTments still hold competitive performance on the SLP; similarly, the architectures found on the SLP also hold comparable performance on the ASSISTments. Note that architecture A5 and S2 have the best generalization to hold the most promising performance on both datasets.

### D. Ablation Study

This section will validate the effectiveness of some devised strategies and analyze the parameter sensitivity. In the following, only the results on the SLP dataset is presented due to higher search cost on the ASSISTments.

To verify the effectiveness of the proposed initialization strategy, we equipped the proposed approach with other two initialization strategies to form two variant approaches, *EMO-NAS-CD (random)* and *EMO-NAS-CD (existing)*. The initial population of the former is randomly generated, and the latter initializes its population purely from existing CDMs. Besides, we also established another variant called *EMO-NAS-CD (crossover+mutation)*, which generates offspring by first applying the *Exchange* operation and then randomly applying one of other three operations. As a result, Fig. 10 presents the convergence profiles of hypervolume (HV) [55] obtained by the proposed approach and its variants. HV measures convergence and diversity of

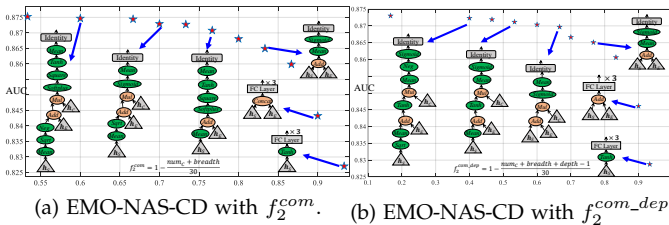


Fig. 11: The non-dominated individuals found by the proposed approach with  $f_2^{com}$  and  $f_2^{com\_dep}$ , and the architecture visualization of six representative individuals.

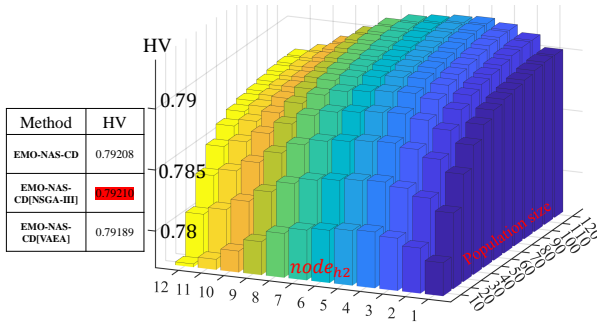


Fig. 12: The influence analysis of hyperparameters ( $Pop$  and  $Node\_range$ ) on EMO-NAS-CD by the HV values.

a population, and a large HV value indicates a good convergence and diversity. The comparison between EMO-NAS-CD and other two variants indicates that the suggested population initialization strategy can indeed speed up the convergence and lead to better final convergence. Besides, we can observe that the proposed genetic operation is significantly better for the proposed approach than the compared genetic operation. The reason behind this is that successively employing two sub-genetic operations to generate offspring will cause major modifications between the generated individuals and their parent individuals, which can promote the exploration of the algorithm but hinder the exploitation of the algorithm to some extent. To sum up, the effectiveness of the proposed initialization and genetic operation can be demonstrated.

To validate the effectiveness of objective  $f_2(\mathcal{A})$  of (5) in assisting the proposed approach to search interpretable CDMs, Fig. 11 exhibits the non-dominated individuals found by two variants of the proposed approach and plots their six representative architectures for observation. Here, the first variant takes the model complexity as the second objective:  $f_2^{com} = 1 - \frac{numc+breadth}{30}$ , and the second variant computes the model complexity as  $f_2^{com\_dep} = 1 - \frac{numc+breadth+depth-1}{30}$ .  $f_2^{com}$  is measured by the sum of the numbers of computation nodes and leaf nodes, and  $f_2^{com\_dep}$  additionally considers the influence of the tree depth (30 is a parameter used for normalizing the objective value). As can be seen from Fig. 11(a), compared to the architectures in the right part, the architectures in the left part have better performance

but at the expense of a much larger increase of depth. Besides, the architectures (located in the upper left area) are much deeper compared to the architectures with similar performance in Fig. 9. The reason behind this is that the objective of model complexity prefers adding a unary operator node, whereas adding a binary operator node would introduce an extra leaf node, leading to a worse objective value. The same observation and conclusion can be drawn from Fig. 11(b), where the found architectures are still very deep. This is because  $f_2^{com\_dep}$  is basically the same as  $f_2^{com}$  yet implicitly assigns a smaller penalty to binary operator nodes, where the assigned penalty is still larger than the penalty assigned to unary operator nodes by  $f_2^{com\_dep}$ . Finally, the effectiveness of the devised model interpretability objective can be validated.

To analyze the sensitivity of the proposed approach to the framework of MOEAs and the hyperparameters  $Pop$  and  $Node\_range$ , Fig. 12 compares HV values on the SLP obtained by EMO-NAS-CD under different hyperparameter combinations of  $Pop$  and  $Node\_range$ . According to Taguchi method [56],  $Pop$  is set from 10 to 120 with step equal to 10, while  $node_{h2}$  in  $Node\_range$  is set from 1 to 12 with step equal to 1 and  $node_{h1}$  is fixed to 2. The original EMO-NAS-CD is under NSGA-II, but EMO-NAS-CD[NSGA-III] and EMO-NAS-CD[VAEA] are EMO-NAS-CD under NSGA-III [57] and VAEA [58], respectively. As can be seen from Fig. 12, firstly, the proposed EMO-NAS-CD is robust to the framework of MOEAs; secondly, the proposed EMO-NAS-CD can obtain relatively good performance when the population size is greater than 80, and it is not necessary to set  $Pop$  to 120 for a slightly higher HV value at the expense of an extra 0.2 times of cost; thirdly, the setting of  $node_{h2}$  has a big influence on the result of the EMO-NAS-CD, and EMO-NAS-CD can obtain relatively good performance when  $node_{h2}$  lies from 3 to 5. Therefore, current hyperparameter settings for EMO-NAS-CD are good enough to some extent.

### E. Discussion

This section will discuss three guidelines for researchers in various domains after the experiments.

The first guideline is for researchers in NAS. To design a task-specific NAS approach, researchers should make the best of their domain knowledge to create a search space. By doing so, the search space can include existing models for the target task and many other potential models. In addition, the search strategy should also be based on the search space's characteristics and the target task's domain knowledge. The second guideline is for researchers in CD, inspiring them on how to design effective CDMs, where the detailed guideline can be found in the last paragraph of Section V-B. The third guideline is for researchers interested in NAS and intelligent education. Considering the success made by our approach, it is promising for other tasks in intelligent

education to employ the NAS technique to design effective neural architectures. Besides, researchers can borrow experiences from this paper to design the objectives of model interpretability, generalization, and robustness, formulate their multiple objectives as a MOP, and then employ a suitable MOEA to solve the MOP.

## VI. CONCLUSION AND FUTURE WORK

In this paper, we proposed to design novel CDMs by leveraging evolutionary multi-objective NAS. Specifically, we first proposed an expressive search space for CD, which contains a large number of potential architectures and existing architectures. Then, we proposed an effective MOGP to search high-performance architectures with high interpretability in the search space by optimizing the MOP having two objectives. To avoid some optimization difficulties, each architecture is first transformed into its corresponding tree architecture and then encoded by tree-based representation for easy optimization. Besides, in the proposed MOGP, an effective genetic operation is designed for offspring generation, and a population initialization strategy is devised to accelerate the convergence. Experimental results demonstrate the superiority of the architectures found by the proposed approach to existing CDMs in terms of performance and model interpretability.

This work has shown the promising prospect of leveraging NAS for CD, but there still exist some threats to the validity of the proposed approach, including internal, external, and construct threats. Firstly, the devised model interpretability objective is the primary internal threat. As seen from Fig. 5, Fig. 8, and Fig. 9, the proposed approach will find relatively different architectures when different model interpretability objectives are adopted. Besides, the proposed model interpretability objective is empirically designed based on some experiences from decision trees, which may limit the emergence of novel architectures as well as the application of found architectures in the real world due to a little unreasonable definition of model interpretability. Therefore, we would like to design more reasonable model interpretability objectives in the future. Secondly, the dataset utilized in the proposed approach is the main external threat. We can find that the found architectures on different datasets are quite different, which indicates that the architectures found by the proposed approach on a single dataset are not general for the cognitive diagnosis task. Besides, the size of the utilized dataset affects the search efficiency of the proposed approach, which leads to an extremely high computation cost when a large-scale dataset is met, e.g., the search cost on ASSISTments is about 15 GPU days. Therefore, in the future, we would like to design generalized CDMs and explore surrogate models [59], [60] to reduce the search cost. Finally, the proposed search space is the main construct threat since it is designed based on the summary of existing architectures and forces all architectures to be single-root trees. Despite high effectiveness, the current search space may

limit the emergence of more potential architectures since CDMs should not always be single-root trees. Therefore, it is interesting to devise other types of search space to contain more effective CDMs.

## REFERENCES

- [1] A. Anderson, D. Huttenlocher, J. Kleinberg, and J. Leskovec, "Engaging with massive online courses," in *Proceedings of the 23rd International Conference on World Wide Web*, 2014, pp. 687–698.
- [2] H. Burns, C. A. Luckhardt, J. W. Parlett, and C. L. Redfield, *Intelligent tutoring systems: Evolutions in design*. Psychology Press, 2014.
- [3] B. P. Woolf, *Student modeling*. Springer, 2010.
- [4] S. Yang, H. Wei, H. Ma, Y. Tian, X. Zhang, Y. Cao, and Y. Jin, "Cognitive diagnosis-based personalized exercise group assembly via a multi-objective evolutionary algorithm," *IEEE Transactions on Emerging Topics in Computational Intelligence*, vol. 7, no. 3, pp. 829–844, 2023.
- [5] J. Beck, "Difficulties in inferring student knowledge from observations (and why you should care)," in *Proceedings of the 13th International Conference of Artificial Intelligence in Education*, 2007, pp. 21–30.
- [6] S. E. Embretson and S. P. Reise, *Item response theory*. Psychology Press, 2013.
- [7] D. L. Torre and J., "Dina model and parameter estimation: A didactic," *Journal of Educational and Behavioral Statistics*, vol. 34, no. 1, pp. 115–130, 2009.
- [8] M. D. Reckase, *Multidimensional item response theory models*. Springer, 2009.
- [9] Y. Koren, R. Bell, and C. Volinsky, "Matrix factorization techniques for recommender systems," *Computer*, vol. 42, no. 8, pp. 30–37, 2009.
- [10] S. Cheng, Q. Liu, E. Chen, Z. Huang, Z. Huang, Y. Chen, H. Ma, and G. Hu, "Dirt: Deep learning enhanced item response theory for cognitive diagnosis," in *Proceedings of the 28th ACM International Conference on Information and Knowledge Management*, 2019, pp. 2397–2400.
- [11] F. Wang, Q. Liu, E. Chen, Z. Huang, Y. Chen, Y. Yin, Z. Huang, and S. Wang, "Neural cognitive diagnosis for intelligent education systems," in *Proceedings of the 2020 AAAI Conference on Artificial Intelligence*, vol. 34, no. 04, 2020, pp. 6153–6161.
- [12] Y. Zhou, Q. Liu, J. Wu, F. Wang, Z. Huang, W. Tong, H. Xiong, E. Chen, and J. Ma, "Modeling context-aware features for cognitive diagnosis in student learning," in *Proceedings of the 27th ACM SIGKDD Conference on Knowledge Discovery & Data Mining*, 2021, pp. 2420–2428.
- [13] W. Gao, Q. Liu, Z. Huang, Y. Yin, H. Bi, M.-C. Wang, J. Ma, S. Wang, and Y. Su, "Rcd: Relation map driven cognitive diagnosis for intelligent education systems," in *Proceedings of the 44th International ACM SIGIR Conference on Research and Development in Information Retrieval*, 2021, pp. 501–510.
- [14] X. Wang, C. Huang, J. Cai, and L. Chen, "Using knowledge concept aggregation towards accurate cognitive diagnosis," in *Proceedings of the 30th ACM International Conference on Information & Knowledge Management*, 2021, pp. 2010–2019.
- [15] H. Ma, J. Zhu, S. Yang, Q. Liu, H. Zhang, X. Zhang, Y. Cao, and X. Zhao, "A prerequisite attention model for knowledge proficiency diagnosis of students," in *Proceedings of the 31st ACM International Conference on Information & Knowledge Management*, 2022, pp. 4304–4308.
- [16] H. Ma, M. Li, L. Wu, H. Zhang, Y. Cao, X. Zhang, and X. Zhao, "Knowledge-sensed cognitive diagnosis for intelligent education platforms," in *Proceedings of the 31st ACM International Conference on Information & Knowledge Management*, 2022, pp. 1451–1460.
- [17] B. Zoph and Q. V. Le, "Neural architecture search with reinforcement learning," *arXiv preprint arXiv:1611.01578*, 2016.
- [18] T. Elsken, J. H. Metzen, and F. Hutter, "Neural architecture search: A survey," *The Journal of Machine Learning Research*, vol. 20, no. 1, pp. 1997–2017, 2019.
- [19] H. Tan, R. Cheng, S. Huang, C. He, C. Qiu, F. Yang, and P. Luo, "Relativenas: Relative neural architecture search via slow-fast learning," *IEEE Transactions on Neural Networks and Learning Systems*, vol. 34, no. 1, pp. 475–489, 2023.

- [20] Y. Sun, B. Xue, M. Zhang, and G. G. Yen, "Completely automated cnn architecture design based on blocks," *IEEE Transactions on Neural Networks and Learning Systems*, vol. 31, no. 4, pp. 1242–1254, 2020.
- [21] H. Liu, K. Simonyan, and Y. Yang, "Darts: Differentiable architecture search," *arXiv preprint arXiv:1806.09055*, 2018.
- [22] Y. Wang, Y. Yang, Y. Chen, J. Bai, C. Zhang, G. Su, X. Kou, Y. Tong, M. Yang, and L. Zhou, "Textnas: A neural architecture search space tailored for text representation," in *Proceedings of the 2020 AAAI Conference on Artificial Intelligence*, vol. 34, no. 05, 2020, pp. 9242–9249.
- [23] A. Baruwa, M. Abisiga, I. Gbadegesin, and A. Fakunle, "Leveraging end-to-end speech recognition with neural architecture search," *arXiv preprint arXiv:1912.05946*, 2019.
- [24] T. Elsken, J. H. Metzen, and F. Hutter, "Efficient multi-objective neural architecture search via lamarckian evolution," *arXiv preprint arXiv:1804.09081*, 2018.
- [25] Y. Zhou, X. Xie, and S.-Y. Kung, "Exploiting operation importance for differentiable neural architecture search," *IEEE Transactions on Neural Networks and Learning Systems*, vol. 33, no. 11, pp. 6235–6248, 2022.
- [26] Y. Liu, Y. Sun, B. Xue, M. Zhang, G. G. Yen, and K. C. Tan, "A survey on evolutionary neural architecture search," *IEEE Transactions on Neural Networks and Learning Systems*, vol. 34, no. 2, pp. 550–570, 2023.
- [27] Z. Lu, I. Whalen, V. Boddeti, Y. Dhebar, K. Deb, E. Goodman, and W. Banzhaf, "Nsga-net: neural architecture search using multi-objective genetic algorithm," in *Proceedings of the 2019 Genetic and Evolutionary Computation Conference*, 2019, pp. 419–427.
- [28] Y. Tian, X. Zhang, C. Wang, and Y. Jin, "An evolutionary algorithm for large-scale sparse multiobjective optimization problems," *IEEE Transactions on Evolutionary Computation*, vol. 24, no. 2, pp. 380–393, 2019.
- [29] S. Li, Y. Sun, G. G. Yen, and M. Zhang, "Automatic design of convolutional neural network architectures under resource constraints," *IEEE Transactions on Neural Networks and Learning Systems*, pp. 1–15, 2021.
- [30] J. Yu, P. Jin, H. Liu, G. Bender, P.-J. Kindermans, M. Tan, T. Huang, X. Song, R. Pang, and Q. Le, "Bignas: Scaling up neural architecture search with big single-stage models," in *Proceedings of the 2020 European Conference on Computer Vision*. Springer, 2020, pp. 702–717.
- [31] Q. Zhou, B. Zhong, X. Liu, and R. Ji, "Attention-based neural architecture search for person re-identification," *IEEE Transactions on Neural Networks and Learning Systems*, vol. 33, no. 11, pp. 6627–6639, 2022.
- [32] B. M. Oloulade, J. Gao, J. Chen, T. Lyu, and R. Al-Sabri, "Graph neural architecture search: A survey," *Tsinghua Science and Technology*, vol. 27, no. 4, pp. 692–708, 2021.
- [33] X. Su, S. You, J. Xie, M. Zheng, F. Wang, C. Qian, C. Zhang, X. Wang, and C. Xu, "Vitas: Vision transformer architecture search," in *Proceedings of the 2021 European Conference on Computer Vision*. Springer, 2022, pp. 139–157.
- [34] B. Feng, D. Liu, and Y. Sun, "Evolving transformer architecture for neural machine translation," in *Proceedings of the 2021 Genetic and Evolutionary Computation Conference Companion*, 2021, pp. 273–274.
- [35] R. Luo, X. Tan, R. Wang, T. Qin, J. Li, S. Zhao, E. Chen, and T.-Y. Liu, "Lightspeech: Lightweight and fast text to speech with neural architecture search," in *Proceedings of the 2021 IEEE International Conference on Acoustics, Speech and Signal Processing*. IEEE, 2021, pp. 5699–5703.
- [36] H. Pham, M. Guan, B. Zoph, Q. Le, and J. Dean, "Efficient neural architecture search via parameters sharing," in *Proceedings of the 2018 International Conference on Machine Learning*. PMLR, 2018, pp. 4095–4104.
- [37] H. Hu, A. Liu, Q. Guan, H. Qian, X. Li, S. Chen, and Q. Zhou, "Adaptively customizing activation functions for various layers," *IEEE Transactions on Neural Networks and Learning Systems*, pp. 1–12, 2022.
- [38] Z. Uykun, "Fast-convergent double-sigmoid hopfield neural network as applied to optimization problems," *IEEE Transactions on Neural Networks and Learning Systems*, vol. 24, no. 6, pp. 990–996, 2013.
- [39] L. Gu, J. Huang, and L. Yang, "On the representational power of restricted boltzmann machines for symmetric functions and boolean functions," *IEEE Transactions on Neural Networks and Learning Systems*, vol. 30, no. 5, pp. 1335–1347, 2019.
- [40] T. Bartz-Beielstein, J. Branke, J. Mehnen, and O. Mersmann, "Evolutionary algorithms," *Wiley Interdisciplinary Reviews: Data Mining and Knowledge Discovery*, vol. 4, no. 3, pp. 178–195, 2014.
- [41] L. Shao, L. Liu, and X. Li, "Feature learning for image classification via multiobjective genetic programming," *IEEE Transactions on Neural Networks and Learning Systems*, vol. 25, no. 7, pp. 1359–1371, 2014.
- [42] Q. Chen, M. Zhang, and B. Xue, "Feature selection to improve generalization of genetic programming for high-dimensional symbolic regression," *IEEE Transactions on Evolutionary Computation*, vol. 21, no. 5, pp. 792–806, 2017.
- [43] Y. Bi, B. Xue, and M. Zhang, "Genetic programming with image-related operators and a flexible program structure for feature learning in image classification," *IEEE Transactions on Evolutionary Computation*, vol. 25, no. 1, pp. 87–101, 2020.
- [44] K. Deb, A. Pratap, S. Agarwal, and T. Meyarivan, "A fast and elitist multiobjective genetic algorithm: Nsga-ii," *IEEE Transactions on Evolutionary Computation*, vol. 6, no. 2, pp. 182–197, 2002.
- [45] O. Maitre, S. Querry, N. Lachiche, and P. Collet, "Esea parallelization of tree-based genetic programming," in *Proceedings of the 2010 IEEE Congress on Evolutionary Computation*. IEEE, 2010, pp. 1–8.
- [46] A. P. Bradley, "The use of the area under the roc curve in the evaluation of machine learning algorithms," *Pattern Recognition*, vol. 30, no. 7, pp. 1145–1159, 1997.
- [47] M. Virgolin, A. De Lorenzo, E. Medvet, and F. Randone, "Learning a formula of interpretability to learn interpretable formulas," in *Proceedings of the 16th International Conference on Parallel Problem Solving from Nature*. Springer, 2020, pp. 79–93.
- [48] Y. Zhang, P. Tiño, A. Leonardis, and K. Tang, "A survey on neural network interpretability," *IEEE Transactions on Emerging Topics in Computational Intelligence*, vol. 5, no. 5, pp. 726–742, 2021.
- [49] D. Hein, S. Udluft, and T. A. Runkler, "Interpretable policies for reinforcement learning by genetic programming," *Engineering Applications of Artificial Intelligence*, vol. 76, pp. 158–169, 2018.
- [50] M. Črepinšek, S.-H. Liu, and M. Mernik, "Exploration and exploitation in evolutionary algorithms: A survey," *ACM Computing Surveys*, vol. 45, no. 3, pp. 1–33, 2013.
- [51] Y. Mu, W. Liu, X. Liu, and W. Fan, "Stochastic gradient made stable: A manifold propagation approach for large-scale optimization," *IEEE Transactions on Knowledge and Data Engineering*, vol. 29, no. 2, pp. 458–471, 2016.
- [52] M. Feng, N. Heffernan, and K. Koedinger, "Addressing the assessment challenge with an online system that tutors as it assesses," *User Modeling and User-adapted Interaction*, vol. 19, no. 3, pp. 243–266, 2009.
- [53] AICFE, "Slp dataset," <https://aic-fe.bnu.edu.cn/en/data/index.html>, 2018.
- [54] J. Derrac, S. García, D. Molina, and F. Herrera, "A practical tutorial on the use of nonparametric statistical tests as a methodology for comparing evolutionary and swarm intelligence algorithms," *Swarm and Evolutionary Computation*, vol. 1, no. 1, pp. 3–18, 2011.
- [55] L. While, P. Hingston, L. Barone, and S. Huband, "A faster algorithm for calculating hypervolume," *IEEE Transactions on Evolutionary Computation*, vol. 10, no. 1, pp. 29–38, 2006.
- [56] J. Sadeghi and S. T. A. Niaki, "Two parameter tuned multi-objective evolutionary algorithms for a bi-objective vendor managed inventory model with trapezoidal fuzzy demand," *Applied Soft Computing*, vol. 30, pp. 567–576, 2015.
- [57] K. Deb and H. Jain, "An evolutionary many-objective optimization algorithm using reference-point-based nondominated sorting approach, part i: solving problems with box constraints," *IEEE Transactions on Evolutionary Computation*, vol. 18, no. 4, pp. 577–601, 2013.
- [58] Y. Xiang, Y. Zhou, M. Li, and Z. Chen, "A vector angle-based evolutionary algorithm for unconstrained many-objective optimization," *IEEE Transactions on Evolutionary Computation*, vol. 21, no. 1, pp. 131–152, 2016.
- [59] Y. Sun, H. Wang, B. Xue, Y. Jin, G. G. Yen, and M. Zhang, "Surrogate-assisted evolutionary deep learning using an end-to-end random forest-based performance predictor," *IEEE Transactions on Evolutionary Computation*, vol. 24, no. 2, pp. 350–364, 2019.
- [60] C. Wei, C. Niu, Y. Tang, Y. Wang, H. Hu, and J. Liang, "Npenas: Neural predictor guided evolution for neural architecture search," *IEEE Transactions on Neural Networks and Learning Systems*, pp. 1–15, 2022.